Nuclear Instruments and Methods in Physics Research A 682 (2012) 59–65

Contents lists available at SciVerse ScienceDirect

Nuclear Instruments and Methods in Physics Research A

journal homepage: www.elsevier.com/locate/nima

Modeling interactions of intermediate-energy neutrons in a plastic scintillator array with GEANT4

Z. Kohley [a,*], E. Lunderberg [b], P.A. DeYoung [b], B.T. Roeder [c,1], T. Baumann [a], G. Christian [a,d], S. Mosby [a,d,2], J.K. Smith [a,d], J. Snyder [a,d], A. Spyrou [a,d], M. Thoennessen [a,d]

[a] National Superconducting Cyclotron Laboratory, Michigan State University, East Lansing, MI 48824, USA
[b] Department of Physics, Hope College, Holland, MI 49423, USA
[c] LPC-Caen, ENSICAEN, IN2P3/CNRS et Université de Caen, 14050 Caen cedex, France
[d] Department of Physics & Astronomy, Michigan State University, East Lansing, MI 48824, USA

ARTICLE INFO

Article history:
Received 1 February 2012
Received in revised form
23 April 2012
Accepted 24 April 2012
Available online 30 April 2012

Keywords:
Monte Carlo simulation
Plastic scintillator array
Neutron detection
GEANT4
Neutron simulation
Cross-talk

ABSTRACT

A Monte Carlo simulation of a large-area neutron time-of-flight detector, built on the GEANT4 framework, has been compared with an experimental measurement of the $^{16}B \rightarrow {}^{15}B + n$ decay produced from a 55 MeV/u ^{17}C beam. The ability of the Monte Carlo simulation to reproduce the intermediate-energy neutron interactions within the detector has been explored using both the stock GEANT4 physics processes and a custom neutron interaction model, MENATE_R. The stock GEANT4 physics processes were unable to reproduce the experimental observables, while excellent agreement was obtained through the inclusion of the MENATE_R model within GEANT4. The differences between the two approaches are shown to be related to the modeling of the neutron–carbon inelastic reactions. Additionally, the use of MENATE_R provided accurate reproduction of experimental signals associated with neutron scattering within the detector. These results provide validation of the Monte Carlo simulation for modeling measurements of multiple neutrons where the identification and removal of false neutron signals, due to multiple neutron scattering, are required.

1. Introduction

An accurate description of neutron interactions at intermediate energies, $\sim 20-300$ MeV, has proven difficult, with previous studies showing inadequacies and inconsistencies between different approaches [1–6]. At energies below 20 MeV, a wealth of data on neutron interaction cross-sections and angular distributions is available and provided by data libraries such as the Evaluated Nuclear Data Files (ENDF) [7,8]. In general, this has allowed for accurate modeling of low energy neutron interactions in various materials; however inconsistencies can still be found [9]. The lack of such an extensive collection of experimental measurements at intermediate energies limits the accuracy of the simulations.

In particular, the varying availability of information on intermediate-energy inelastic reactions has lead to the use of cascade models within simulation packages such as GEANT4 [10,11]. Thus, the partitioning of the different discrete inelastic reaction channels is calculated within the cascade models, which are tuned to reproduce specific experimental observables, rather than being based on experimentally determined cross-sections. While this has proven useful for certain applications [12], cases where the simulated system is particularly sensitive to specific reaction channels require more realistic modeling. Therefore, the sparse but available experimental inelastic reaction data has been compiled for specific materials, such as carbon [13], allowing for models based solely on experimental cross-sections to be developed [1,4,14]. Comparison of the cascade models and the cross-section driven approaches at intermediate energies will continue to help advance our ability to accurately model neutron interactions.

Improved simulations of intermediate-energy neutrons are of specific interest for exploring neutron unbound states of nuclei at and beyond the neutron dripline, which often requires coincidence neutron–fragment detection. Understanding and exploring the structure of nuclei is one of the fundamental goals of nuclear science and the production of radioactive-ion beams has opened the door for measurements from the proton to neutron dripline for the lighter elements [15–17]. The Modular Neutron Array (MoNA) [18,19] is a large-area neutron detector which has been used to measure the unbound states of nuclei using the invariant-mass technique. At the National Superconducting Cyclotron Laboratory (NSCL) at the Michigan State University, the optimum beam energy to produce and subsequently study nuclei near the

* Corresponding author.
E-mail address: zkohley@gmail.com (Z. Kohley).
[1] Present Address: Cyclotron Institute, Texas A&M University, College Station, TX 77843, USA.
[2] Present Address: Los Alamos National Laboratory, Los Alamos, NM 87545, USA.

0168-9002/$ - see front matter © 2012 Elsevier B.V. All rights reserved.
http://dx.doi.org/10.1016/j.nima.2012.04.060

neutron dripline with MoNA and the Sweeper dipole magnet is $\sim 45-85$ MeV/u. The neutrons emitted from the decay of the unbound nuclei of interest will, therefore, have a similar range of energies. An accurate description of the interactions of these intermediate-energy neutrons is required in order to have a robust model of MoNA.

As studies using MoNA have expanded to examine two neutron unbound states [20,21], it has become increasingly important to have an accurate description of the scattering of neutrons within the detector. For example, an event with two detected interactions could correspond to either a single neutron scattering twice in the detector array or the actual measurement of two separate neutrons. A proper experimental measurement will require the discrimination between these two different scenarios. The experimental results will then depend on the ability of the simulation to correctly model the neutron scattering and discrimination cuts. Additionally, understanding the interactions of intermediate-energy neutrons and therefore improving the modeling capabilities would benefit any application involving intermediate-energy neutrons. For example, experiments measuring intermediate-energy neutrons emitted from heavy-ion collisions have provided constraints on the nuclear equation of state [22]. Also, there is significant interest in simulating and measuring the interactions of fast secondary neutrons produced during heavy-ion therapy [23–27].

In this paper, a Monte Carlo simulation, built on the GEANT4 framework, of the MoNA detector is compared with experimental data. Within the simulation we compare the standard GEANT4 physics models with a custom neutron interaction model, MENATE_R [28]. Details about the MoNA detector setup and the experiment used for validation of the simulation are provided in Sections 2 and 3, respectively. In Section 4 descriptions of the simulation and custom physics model MENATE_R are provided. The results of the simulations and a comparison with experimental data are shown in Section 5. Lastly, the conclusions are presented in Section 6.

2. Modular neutron array (MoNA)

The modular neutron array (MoNA) consists of 144 plastic scintillator bars [18,19]. As shown in Fig. 1, nine walls, of 16 bars each, were placed 790 cm from the target position for the examined experiment (Section 3). Each bar is 200 cm × 10 cm × 10 cm and is made from BC-408 material. Light is produced in the plastic scintillator bars, mostly, from the elastic scattering of neutrons on hydrogen nuclei. The light produced from recoil carbon nuclei is much less and often not detected. A light guide and photomultiplier tube (PMT) are attached to the end of each bar for light collection and detection. The position of the neutron interaction is determined from the discrete positions of each bar in the array and the interaction point within the bar which is calculated from difference in the time for the light to reach the PMTs. The total deposited energy, represented by the amount of light produced, is also recorded. The kinetic energy of the neutrons is determined from the time-of-flight between a timing scintillator placed in front of the reaction target and MoNA, as shown in Fig. 1.

While MoNA provides information on the neutrons, the coincident charged breakup products are analyzed in a suite of charged-particle detectors after being deflected by the large-gap 4-Tm superconducting sweeper magnet [29]. Cathode readout drift chambers (CRDCs) provide tracking information which allow for the fragments to be inverse tracked through the sweeper magnet back to the target [30]. The energy-loss in the ionization chamber and a thick total energy scintillator provide charge identification of the fragment, while the mass is determined from a corrected time-of-flight between the reaction target and a thin timing scintillator [31,32].

3. Experiment

In order to benchmark the accuracy of the Monte Carlo simulation, a "clean" experimental data set is required for comparison. Ideally this would be a case where only a single neutron is impinging on the neutron detector. The measurement of the ground state of ^{16}B by Spyrou et al. [33] was chosen for this reason. The Coupled Cyclotron Facility at the NSCL produced a 55 MeV/u ^{17}C beam, from a 120 MeV/u ^{22}Ne primary beam, which impacted a 470 mg/cm^2 ^{9}Be reaction target. A one-proton knockout reaction populated the ground state of the unbound ^{16}B nucleus, which immediately decayed into ^{15}B + n. For each detected ^{15}B fragment there should only be a single neutron in coincidence. Therefore, any multiple interaction events observed in MoNA must correspond to the multiple scattering of the single neutron and should allow for a detailed comparison with the simulation.

4. Monte Carlo simulation

The Monte Carlo simulation for the MoNA+Sweeper setup is built in two parts based on the propagation of (1) the charged fragment through the sweeper magnet and (2) the neutron

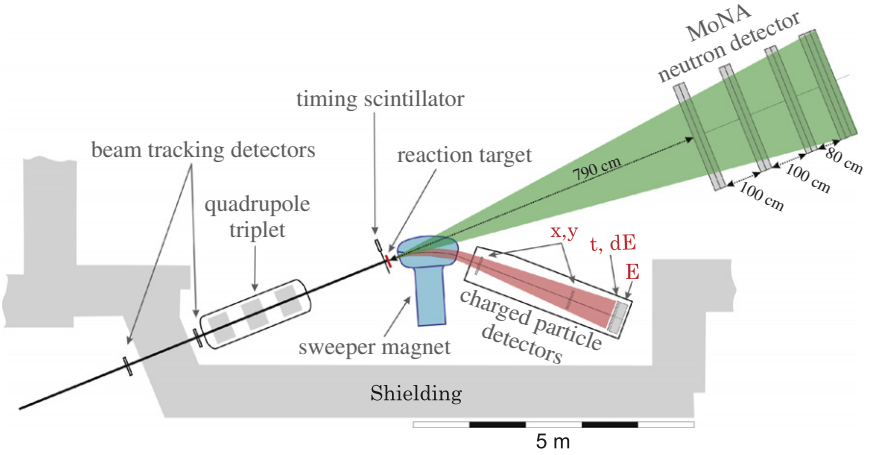

Fig. 1. Schematic of the sweeper magnet and modular neutron array (MoNA) configuration from the ^{16}B experiment [33].

in MoNA. The one-proton knockout reaction with the ^{17}C beam impinging on the ^{9}Be target was simulated within the Glauber model. The decay of the resulting unbound ^{16}B nucleus was modeled according to the decay energy line-shape observed in Ref. [33]. The ^{15}B fragment, from the decay of ^{16}B, was then tracked through the sweeper magnet [30]. The required tracking maps were created from the ion-optics COSY Infinity program [34] which produces forward (inverse) ion-optical matrices allowing for the position and angle of the fragments at the charged particle detector (target) to be reconstructed from the position and angle at the target (charged particle detector). The same magnetic field map and tracking algorithms used for the experiment were applied to the simulation. The ^{15}B fragment was then propagated through the charged particle detectors, accounting for all experimental acceptances and resolutions.

MoNA and the sweeper magnet were both constructed within the GEANT4 toolkit (version 9.4.p01) [10,11]. The light guides, vinyl wrapping, and BC-408 material were all included in the modeling of the MoNA bars. The BC-408 material was created with the nominal hydrogen to carbon ratio of 1.104 and a density of 1.032 g/cm^3. After the simulated ^{16}B decay, the angle and energy of the neutron was passed into GEANT4 which then propagated the neutron through the gap of the sweeper magnet and into MoNA. While the neutron propagation was modeled within GEANT4, the propagation of the residual charged fragment (^{15}B), as discussed above, was completed in a separate code for ease with using the COSY Infinity tracking maps . As the neutron interacted with the carbon and hydrogen, the energy deposited in the detector bars was converted into a light output using Birks formula [35] and summed. The position, light output, and time-of-flight of each neutron interaction were recorded, matching the signals recorded in the experiment. The detector thresholds were also incorporated into the simulation. By combining the simulated propagation of the ^{15}B fragment through the sweeper setup with the GEANT4 description of the neutron interactions in MoNA, an accurate comparison can be made between the Monte Carlo simulation and the experimental data.

4.1. Modeling neutron interactions

GEANT4 provides a flexible framework to explore different physics models which describe the interaction of particles in a material of interest. There is a distinct change in the neutron transport models available in GEANT4 above and below 20 MeV. Below 20 MeV, GEANT4 has high precision neutron transport models (*G4NeutronHPElastic* and *G4NeutronHPInelastic*) available for all materials [36]. The high precision models are based on the Evaluated Nuclear Data Files (ENDF/B-VI) [7,8] which contains tabulated cross-sections below 20 MeV for elastic reactions and the different inelastic final states, such as nγ, np, nd, nt, nα, n2α, etc. The high-quality ENDF/B-VI data generally allows for accurate simulations of these low-energy neutrons.

As mentioned above, the optimum energy for producing radioactive ion beams at the NSCL combined with the 4-Tm bending power limit of the sweeper magnet defines the projectile energy range for experiments with MoNA to be $\sim$45$-$85 MeV/u. Therefore, the neutron energy range of interest is $\sim$30$-$100 MeV. While the high precision transport models are included in our GEANT4 simulation, the modeling of neutrons above 20 MeV is of larger importance.

In Section 5 two different methods for describing the intermediate-energy neutron interactions within the MoNA detector are compared. The first method will be referred to as G4-Physics, since it uses stock GEANT4 physics classes to model the $>$20 MeV neutrons. This includes the *G4HadronElasticProcess* and *G4LElastic* classes for the elastic scattering of the neutron off the carbon and hydrogen nuclei. The inelastic reactions between the neutron and carbon nuclei were simulated with the GEANT4 cascade model [36], included through the *G4LENeutronInelastic* and *G4CascadeInterface* classes. The GEANT4 cascade model includes the Bertini intranuclear cascade model [12] with excitons followed by a pre-equilibrium decay. Following the pre-equilibrium model, the excited residual nucleus is cooled using a nuclear breakup, evaporation, or fission model [36]. Neutron interaction cross-sections from the high-energy Japanese Evaluated Data Library (JENDL-HE) [37,38] were used for both the elastic and inelastic reactions and were implemented by the *G4NeutronHPJENDLHEElasticData* and *G4NeutronHPJENDLHEInelasticData* classes. The JENDL-HE cross-sections, which range from 20 MeV to 3 GeV, for the elastic and inelastic neutron reactions on hydrogen and carbon are shown in Figs. 2 and 3.

In comparison to the G4-Physics, a custom neutron interaction model, referred to as MENATE_R [28], was incorporated into the GEANT4 framework. MENATE_R is based on the original FORTRAN neutron simulation code MENATE [14], which was used to simulate neutron interactions within NE213 scintillators. As part of the EURISOL design study [28], the original code was developed into a C++ class derived from the *G4VDiscreteProcess* class which allowed for the code to be easily incorporated into GEANT4. Thus, the transport of the neutron, along with any other particles, through the MoNA+sweeper setup is still handled by GEANT4,

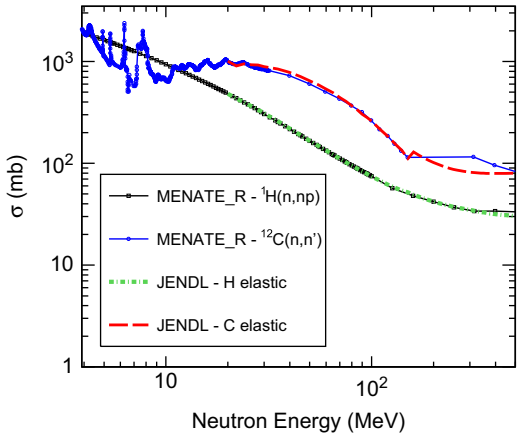

Fig. 2. Elastic neutron–hydrogen and neutron–carbon reaction cross-sections, as a function of the incident neutron energy, used in the MENATE_R and G4-Physics (JENDL) models.

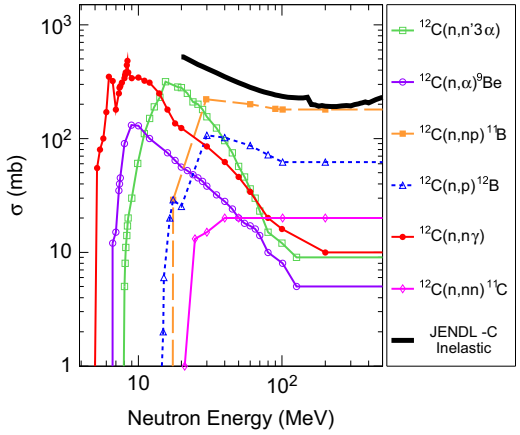

Fig. 3. Inelastic neutron–carbon reaction cross-sections are shown as a function of the incident neutron energy. MENATE_R uses the six different discrete reaction channel cross-sections while the G4-Physics uses the total inelastic reaction cross-sections taken from the JENDL-HE library [37].

yet the cross-sections and kinematics of the neutron interactions are provided by the MENATE_R code. The elastic and inelastic neutron cross-sections used within MENATE_R are shown in Figs. 2 and 3. The elastic reaction cross-sections above 20 MeV and the discrete carbon inelastic cross-section are from Refs. [13,1] (and references therein). Below 20 MeV the elastic cross-section data are taken from the ENDF/B-VI database [7,8].

As shown in Fig. 2, the cross-sections used by MENATE_R and G4-Physics (JENDL) for the elastic neutron interactions with hydrogen and carbon are very similar over the region of interest. The most significant difference between MENATE_R and the G4-Physics is the description of the neutron–carbon inelastic reactions. MENATE_R treats the inelastic interactions with carbon as a set of discrete reactions channels with cross-sections derived from experimental data, as shown in Fig. 3. In comparison, G4-Physics uses the total inelastic neutron–carbon cross-sections, from JENDL-HE, and then applies the GEANT4 cascade model to simulate the out-going reaction channel. Thus, the G4-Physics depends on the accuracy of the GEANT4 cascade model's description of neutron–carbon interactions, whereas MENATE_R is dependent only on the accuracy and availability of the experimental data. One limitation of the approach of MENATE_R is that it requires the input of cross-sections for the discrete reaction channels which are not widely available at intermediate energies for a large variety of materials. Currently, this limits the use of MENATE_R to hydrocarbon-based detectors, such as MoNA.

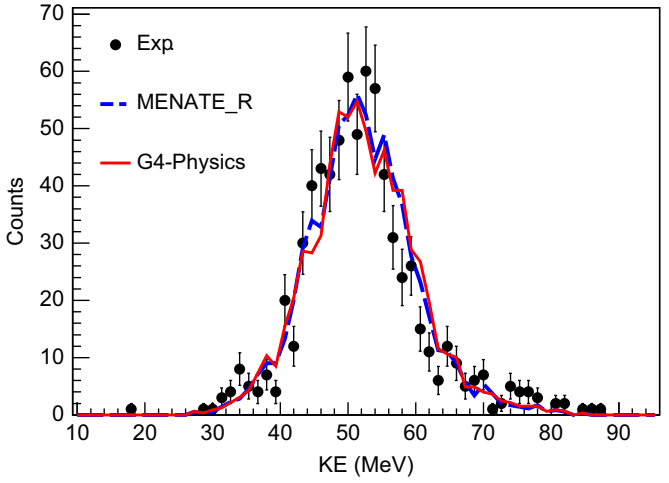

Fig. 4. Measured neutron kinetic energy (KE) distribution from the ^{16}B experiment [33] compared with the Monte Carlo simulation using the MENATE_R and G4-Physics models. The simulated distributions have been normalized to the total area of the experimental distribution.

5. Results and discussion

The kinetic energy (KE) of the neutron emitted from the decay of ^{16}B will be defined by the one-proton knockout reaction kinematics, the energy loss of the ^{17}C projectile in the target, and the decay energy distribution. In Fig. 4 the KE distribution of the first time-ordered interaction in MoNA, in coincidence with the detection of a ^{15}B fragment, is presented. The results show that 30–70 MeV neutrons are produced from the 55 MeV/u reaction. The KE distributions from the G4-Physics and MENATE_R simulations are nearly identical since the distributions are determined by the reaction and decay kinematics. The agreement between the Monte Carlo simulation and experiment demonstrates that the reaction and decay ($_{17}$C(−p)→$_{16}$B→$_{15}$B+n) is being properly modeled.

One simple, but very important, observable for the Monte Carlo simulation to reproduce is the multiplicity distribution of interactions in MoNA. In each event a single neutron is impinging on MoNA, and therefore the observation of multiple interactions must be associated with the original neutron scattering within the detector producing multiple signals and/or the production of secondary particles which can then interact within the array. Fig. 5(a) presents the multiplicity distribution of interactions observed in the experiment in comparison to the simulation with the MENATE_R and G4-Physics models. The experimental data shows a rapid decrease in the number of observed events as a function of increasing multiplicity. In the majority of experimental events only a single interaction was recorded. The G4-Physics simulation strongly overproduced the number of high multiplicity events relative to the multiplicity = 1 events. In comparison, the simulation, with the inclusion of the MENATE_R, very closely matches the experimental multiplicity distribution.

In addition to the multiplicity distribution, the deposited energy in the detector bars provides another test of the neutron interaction models. As discussed above, the deposited energy is measured as the amount of light produced from the interaction of the neutron with the hydrogen or carbon nuclei. In Fig. 5(b) the energy distribution from the G4-Physics and MENATE_R simulations are compared with the experiment. Again, the MENATE_R model shows good agreement with the experimental distribution. The

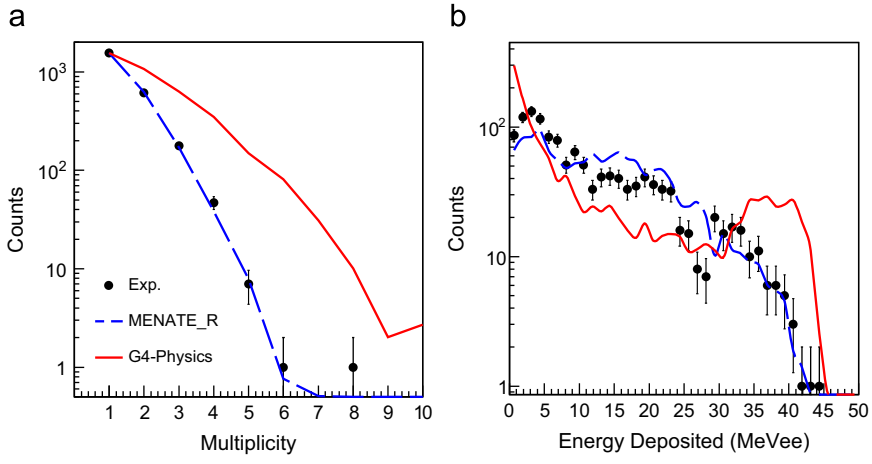

Fig. 5. The experimental (a) multiplicity and (b) deposited energy distributions are compared to the Monte Carlo simulation using the MENATE_R and G4-Physics models. The simulated (a) multiplicity distributions were scaled to match the number of multiplicity = 1 experimental events. The simulated (b) deposited energy distributions were normalized to the total area of the experimental distribution.

use of the G4-Physics causes an overproduction of both the low and high energy signals in the detector. Together Figs. 5(a) and (b) clearly indicate that the stock G4-Physics models are unable to accurately describe the interaction of the intermediate-energy neutrons with the hydrocarbon scintillator bars of MoNA.

Since the multiplicity and deposited energy distributions are produced from all the interactions in MoNA, whether induced by a neutron or secondary particle, and the neutron–hydrogen and neutron–carbon elastic cross-sections used in the G4-Physics and MENATE_R are very similar (Fig. 2), the differences in the description of the inelastic neutron–carbon reactions are likely responsible for the large discrepancies observed between the two models. As mentioned in Section 4, MENATE_R treats the inelastic reactions as a set of discrete channels based on experimental cross-section measurements, while the G4-Physics uses the GEANT4 cascade model to simulate the interaction between the neutron and carbon nucleus.

To demonstrate the differences in the two approaches to modeling the inelastic reactions, the multiplicity distributions of secondary γ-ray interactions in MoNA was compared and is shown in Fig. 6. The ^{12}C(n,nγ) channel is particularly important because the produced γ rays can propagate to other detector bars and produce additional interactions in the array. As shown in Fig. 6, there is a drastic difference in the number of γ rays produced and subsequently interacting with the detector bars between the MENATE_R and G4-Physics approaches. It is important to note that in the distributions presented in Fig. 6 the experimental thresholds were not applied, therefore each γ-ray interaction does not necessarily correspond to a valid signal in the detector. The results show that secondary γ rays are produced and interact with the MoNA detector in only ∼10% of the simulated events when using MENATE_R in comparison to ∼70% with the G4-Physics. This large overestimation of the production of γ rays from the GEANT4 cascade could cause an increased number of low-energy interactions and multiplicity >1 events, both of which were observed in Fig. 5. It is important to note that the differences observed in the γ-ray production, while drastic, are likely not the sole cause for the discrepancies shown in Fig. 5 but rather present a clear example of the differences between the G4-Physics and MENATE_R.

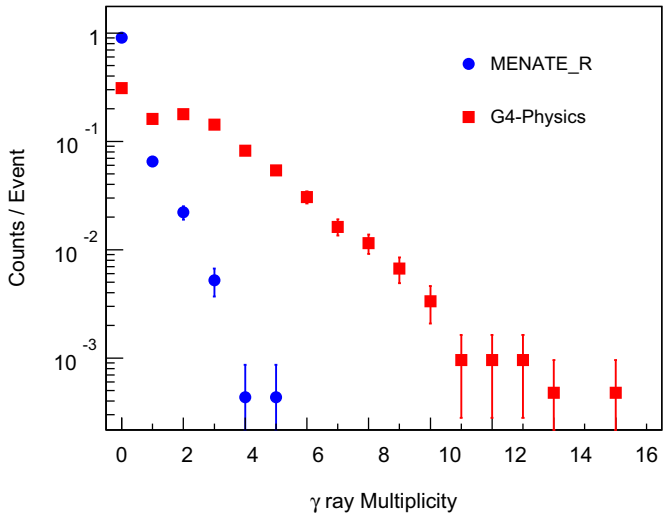

Fig. 6. Multiplicity distribution for interactions in MoNA from γ rays produced from inelastic neutron–carbon reaction in the Monte Carlo simulation with the MENATE_R and G4-Physics neutron interaction models.

From the discussion and results presented above it is clear that the G4-Physics is unable to accurately reproduce and describe the neutron interactions at the examined intermediate energies. In the following, additional comparisons are presented between the experimental data and the Monte Carlo simulation using only the MENATE_R model to provide validation for use in future studies. In particular, it is important to examine events with multiple interactions in MoNA as these events should prove more difficult for the simulation to reproduce.

In Fig. 7 the spatial distribution of interactions in the *X*, *Y*, and *Z* directions, for events with a multiplicity >1, is shown. The *Y* and *Z* positions of a interaction are determined by the position of the MoNA bar and therefore are discrete values. As shown in Fig. 1, the nine walls of MoNA were in a split-configuration in the *Z* direction leading to the distribution observed in Fig. 7(c). The interaction point within each bar, *X* position, is determined from the relative time difference measured between the ends of the bar. The *X*-position distribution is off-center due to the $B\rho$ setting of the sweeper magnet, which produced a biased angular acceptance for the ^{15}B fragments. However, this feature was accounted for in the simulation since the experimental magnetic field map was used, which allowed for the off-center *X* position distribution to be reproduced. Overall, the experimental and simulated distributions show reasonable agreement.

In events with multiple interactions, the distance, angle, and velocity between the first and second interaction is representative

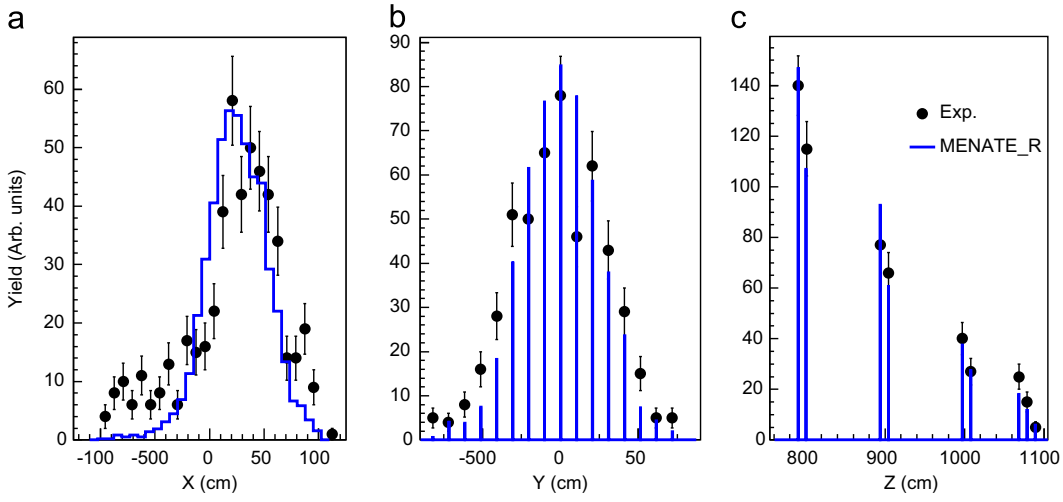

Fig. 7. Spatial distributions in the *X*, *Y*, and *Z* directions from the experiment are compared with the Monte Carlo simulation using MENATE_R in panels (a), (b), and (c), respectively. The simulated distributions were normalized to the total area of the experimental distributions.

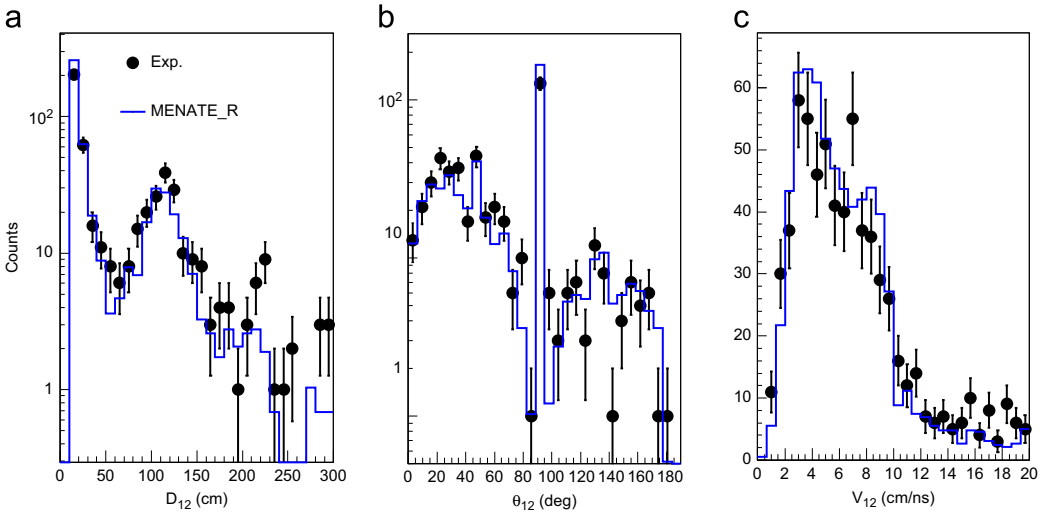

Fig. 8. Relative (a) distance, (b) angle, and (c) velocity between the first and second interaction in MoNA from the experiment is compared with the Monte Carlo simulation with the MENATE_R neutron interaction model. The simulated distributions were normalized to the total area of the experimental distributions.

of the neutron scattering properties. In measuring 2-neutron (2n) decays with MoNA it becomes important to be able to differentiate a true 2n event from an event where the first and second interaction are both produced by a single neutron, often referred to as cross-talk. A current method for removing false 2n events, or cross-talk, involves placing cuts on the relative distance and velocity of the first and second interactions [39,40] (more detailed studies of cross-talk removal can be found in Refs. [41–43]). In Fig. 8 the relative distance (D_{12}), angle (θ_{12}), and velocity (V_{12}) between the first and second interaction are shown for both the experimental and simulated data. The relative velocity is defined as $V_{12}=(D_{12})/(t_2-t_1)$, where $t_1(t_2)$ is the time-of-flight of the first(second) interaction. Excellent agreement is found between the simulated and experimental distributions for the different observables. The large number of events with a small D_{12} and $\theta_{12}=90^\circ$ indicates that a scattered neutron will most likely interact within the same wall of MoNA. Additionally, the small number of events with V_{12} greater than the beam velocity, ~ 10 cm/ns, demonstrates that it is very unlikely that the second interaction would produce a larger measured velocity than the first interaction. While not presented in Figs. 7 and 8, the G4-Physics simulations shows similar agreement to the experimental data as MENATE_R except for the V_{12} distribution. The G4-Physics simulation is unable to reproduce the V_{12} distribution due to an additional peak around $V_{12}=30$ cm/ns, which is related to the overproduction of γ rays that would produce events where two successive hits would have a relative velocity near the speed of light. The accuracy of these results provide validation that simulation can describe the scattering and multiple interactions of a neutron in MoNA.

6. Conclusions

The ability to accurately model intermediate-energy neutrons within the MoNA detector has been explored using the GEANT4 toolkit. The use of the stock neutron cross-sections and physics models included in GEANT4 (G4-Physics) were compared to a custom neutron interaction code (MENATE_R), which was incorporated into the GEANT4 framework. The Monte Carlo simulations were compared to an experimental measurement of the decay of $^{16}\mathrm{B}\rightarrow{}^{15}\mathrm{B}+\mathrm{n}$.

Drastic differences in the interaction multiplicity and deposited energy distributions were observed between the G4-Physics and MENATE_R neutron interaction models. While the MENATE_R physics model accurately reproduced the experimental distributions, the G4-Physics overproduced multiple interaction events and was unable to reproduce the experimental deposited energy distributions. These differences are attributed to the different approaches taken in the modeling of the inelastic neutron–carbon reactions. This corroborates the results of the benchmarking of MENATE_R against data for liquid scintillator detectors for energies around 100 MeV [28]. In MENATE_R the inelastic reactions are modeled as discrete reaction channels based on experimental information, while the G4-Physics uses a cascade model to determine the partition of the outgoing reaction channels. While the MENATE_R approach requires a more extensive collection of experimental data, the benefits of such an approach are clearly shown in the presented results and indicate a need for future experimental efforts to measure discrete inelastic reaction channels for intermediate-energy neutrons. Future studies using other neutron transport simulations, such as FLUKA [44,45] and MCNPX [46], would be of great interest as they use different models for the inelastic reactions and may provide insight into improving the accuracy of the calculations.

Additionally, the relative distance, angle, and velocity distributions, calculated from the first and second interactions, from the MENATE_R simulation showed excellent agreement with the experimental distributions. These observables are particularly important as they are often used to discriminate between true and false two neutron events. In general, the results presented above for the MoNA Monte Carlo simulation, using GEANT4+MENATE_R, demonstrate impressive accuracy in reproducing the experimental observables and provide confidence in simulating measurements requiring the detection of multiple neutrons.

Acknowledgments

This material is based upon work supported by the Department of Energy National Nuclear Security Administration under Award Number(s) DE-NA0000979. This work was also supported by the National Science Foundation under grant No PHY06-06007 and PHY11-02511. One of the authors (BR) acknowledges the financial support of the European Community under the FP6 EURISOL-DS project (contract no 515768). He also wishes to thank his colleagues FM Marqués, JL Lecouey and NA Orr from LPC-Caen for their aid in the development of MENATE_R.

This report was prepared as an account of work sponsored by an agency of the United States Government. Neither the United States Government nor any agency thereof, nor any of their

employees, makes any warranty, express or implied, or assumes any legal liability or responsibility for the accuracy, completeness, or usefulness of any information, apparatus, product, or process disclosed, or represents that its use would not infringe privately owned rights. Reference herein to any specific commercial product, process, or service by trade name, trademark, manufacturer, or otherwise does not necessarily constitute or imply its endorsement, recommendation, or favoring by the United States Government or any agency thereof. The views and opinions of authors expressed herein do not necessarily state or reflect those of the United States Government or any agency thereof.

References

[1] R.A. Cecil, B.D. Anderson, R. Madey, Nuclear Instruments and Methods in Physics Research Section A 161 (1979) 439.
[2] S. Meigo, Nuclear Instruments and Methods in Physics Research Section A 401 (1997) 365.
[3] I. Tilquin, et al., Nuclear Instruments and Methods in Physics Research Section A 365 (1995) 446.
[4] R.C. Byrd, W.C. Sailor, Nuclear Instruments and Methods in Physics Research Section A 274 (1989) 494.
[5] M.W. McNaughton, F.P. Brady, W.B. Broste, A.L. Sagle, S.W. Johnsen, Nuclear Instruments and Methods in Physics Research Section A 116 (1974) 25.
[6] M.W. McNaughton, N.S.P. King, F.P. Brady, J.L. Ullman, Nuclear Instruments and Methods in Physics Research Section A 129 (1975) 241.
[7] P. Rose (Ed.), ENDF/B-VI Summary Document, Report BNL-NCS-17541, National Nuclear Data Center, Brookhaven National Laboratory, 1991.
[8] Evaluated Nuclear Data File (ENDF) 〈http://www.nndc.bnl.gov/exfor/endf00.jsp〉.
[9] C. Guardiola, K. Amgarou, F. Garcíac, C. Fleta, D. Quirion, M. Lozano, Journal of Instrumentation 6 (2011) T09001.
[10] S. Agostinelli, J. Allision, K. Amako, J. Apostolakis, H. Araujo, P. Arce, M. Asai, D. Axen, S. Banerjee, G. Barrand, F. Behner, L. Bellagamba, J. Boudreau, et al., Nuclear Instruments and Methods in Physics Research Section A 506 (2003) 250.
[11] J. Allision, K. Amako, J. Apostolakis, H. Araujo, P.A. Dubios, M. Asai, G. Barrand, R. Capra, S. Chauvie, R. Chytracek, G.A.P. Cirrone, G. Cooperman, et al., IEEE Transaction on Nuclear Science NS-53 (2006) 270.
[12] A. Heikkinen, N. Stepanov, J.P. Wellisch, in: Proceedings of 2003 Conference for Computing in High-Energy and Nuclear Physics (CHEP 03), 2003, arXiv:nucl-th/0306008.
[13] A. Del Guerra, Nuclear Instruments and Methods in Physics Research Section A 135 (1976) 337.
[14] P. Desesquelles, A.J. Cole, A. Dauchy, A. Giorni, D. Heuer, A. Lleres, C. Morand, J. Sain-Martin, P. Stassi, J.B. Viano, B. Chambon, B. Cheynis, D. Drain, C. Pastor, Nuclear Instruments and Methods in Physics Research Section A 307 (1991) 366.
[15] T. Baumann, A. Spyrou, M. Thoennessen, Reports on Progress in Physics.
[16] B. Jonson, Phys. Rep. 389 (2004) 1.
[17] B.A. Brown, Progress in Particle and Nuclear Physics 47 (2001) 517.
[18] B. Luther, T. Baumann, M. Thoennessen, J. Brown, P. DeYoung, J. Finck, J. Hinnefeld, R. Howes, K. Kemper, P. Pancella, G. Peaslee, W. Rogers, S. Tabor, Nuclear Instruments and Methods in Physics Research Section A 505 (2003) 33.
[19] T. Baumann, et al., Nuclear Instruments and Methods in Physics Research Section A 543 (2005) 517.
[20] E. Lunderberg, P.A. DeYoung, Z. Kohley, H. Attanayake, T. Baumann, D. Bazin, G. Christian, D. Divaratne, S.M. Grimes, A. Haagsma, J.E. Finck, N. Frank, et al., Physics Review Letters 108 (2012) 142503.
[21] A. Spyrou, Z. Kohley, T. Baumann, D. Bazin, B.A. Brown, G. Chrstian, P.A. DeYoung, J.E. Finck, N. Frank, E. Lunderberg, S. Mosby, W.A. Peters, A. Schiller, J.K. Smith, J. Synder, M.J. Strongman, M. Thoennessen, A. Volya, Physics Review Letters 108 (2012) 102501.
[22] M.A. Famiano, T. Liu, W.G. Lynch, M. Mocko, A.M. Rogers, M.B. Tsang, M.S. Walace, R.J. Charity, S. Komarov, G.G. Sarantites, L.G. Sobotka, G. Verde, Physics Review Letters 97 (2006) 052701.
[23] S. Yonai, N. Matsufuji, T. Kanai, Medical Physics 36 (2009) 4830.
[24] K. Gunzert-Marx, D. Schardt, R.S. Simon, Radiotherapy and Oncology 73 (2004) S92.
[25] I. Pshenichnov, I. Mishustin, W. Greiner, Physics in Medicine and Biology 50 (2005) 5493.
[26] B. Dang, W. Li, J. Wang, Radiation Protection Dosimetry 117 (2005) 369.
[27] Y. Uozumi, et al., Progress in Nuclear Science and Technology 1 (2011) 114.
[28] B. Roeder, Development and Validation of Neutron Detection Simulations for EURISOL, EURISOL Design Study, Report: [10-25-2008-006-In-beamvalidations.pdf, pp 31-44] (2008). URL: 〈www.eurisol.org/site02/physics_and_instrumentation/〉.
[29] M.D. Bird, S.J. Kenney, J. Toth, H.W. Weijers, J.C. DeKamp, M. Thoennessen, A.F. Zeller, IEEE Transactions on Applied Superconductivity 15 (2005) 1252.
[30] N. Frank, A. Schiller, D. Bazin, W.A. Peters, M. Thoennessen, Nuclear Instruments and Methods in Physics Research Section A 580 (2007) 1478.
[31] N. Frank, T. Baumann, D. Bazin, B.A. Brown, J. Brown, P.A. DeYoung, J.E. Finck, A. Gade, J. Hinnefeld, R. Howes, J.L. Lecouey, B. Luther, W.A. Peters, H. Scheit, A. Schiller, M. Thoennessen, J. Tostevin, Nuclear Physics A 813 (2008) 199.
[32] A. Schiller, N. Frank, T. Baumann, D. Bazin, B.A. Brown, J. Brown, P.A. DeYoung, J.E. Finck, A. Gade, J. Hinnefeld, R. Howes, J.L. Lecouey, B. Luther, W.A. Peters, H. Scheit, M. Thoennessen, J.A. Tostevin, Physics Review Letters 99 (2007) 112501.
[33] A. Spyrou, T. Baumann, D. Bazin, G. Blanchon, A. Bonaccorso, E. Breitbach, J. Brown, G. Christian, A. DeLine, P.A. DeYoung, J.E. Finck, N. Frank, S. Mosby, W.A. Peters, A. Russel, A. Schiller, M.J. Strongman, M. Thoennessen, Physics Letters B 683 (2010) 129.
[34] K. Makino, M. Berz, Nuclear Instruments and Methods in Physics Research Section A 558 (2005) 346.
[35] G.F. Knoll, Radiaton Detection and Measurement, John Wiley & Sons, Inc., 2000.
[36] Geant4 Physics Reference Manual. 〈http://geant4.web.cern.ch〉, 2011.
[37] Y. Watanabe, et al., Nuclear data evaluations for JENDL high-energy file, in: Proceedings of the International Conference on Nuclear Data for Science and Technology, vol. 769, AIP Conference Proceedings, 2005, p. 326.
[38] Japanese Evaluated Nuclear Data Library (JENDL). 〈http://wwwndc.jaea.go.jp/jendl/jendl.html〉.
[39] C.R. Hoffman, T. Baumann, J. Brown, P.A. DeYoung, J.E. Finck, N. Frank, J.D. Hinnefeld, S. Mosby, W.A. Peteres, W.F. Rogers, A. Schiller, J. Snyder, A. Spyrou, S.L. Tabor, M. Thoennessen, Physics Review C 83 (2011) 031303. (R).
[40] T. Nakamura, et al., Physics Review Letters 96 (2006) 252502.
[41] J. Wang, A. Galonsky, J.J. Kruse, P.D. Zecher, F. Deak, A. Horvath, A. Kiss, Z. Seres, K. Ieki, Y. Iwata, Nuclear Instruments and Methods in Physics Research Section A 397 (1997) 380.
[42] F.M. Marques, M. Labiche, N.A. Orr, F. Sarazin, J.C. Angelique, Nuclear Instruments and Methods in Physics Research Section A 450 (2000) 109.
[43] J. Ljungvall, M. Palacz, J. Nyberg, Nuclear Instruments and Methods in Physics Research Section A 528 (2004) 741.
[44] G. Battistonie, S. Muraro, P.R. Sala, F. Cerutti, A. Ferrari, S. Roesler, A. Fasso, J. Ranft, AIP Conference Proceedings 896 (2007) 31.
[45] FLUKA 〈http://www.fluka.org〉.
[46] MCNPX 〈mcnpx.lanl.gov〉.